NANO LETTERS

Letter

pubs.acs.org/NanoLett

Scaling Properties of Charge Transport in Polycrystalline Graphene

Dinh Van Tuan,[†] Jani Kotakoski,[*,§,∥] Thibaud Louvet,[†,⊥] Frank Ortmann,[†] Jannik C. Meyer,[§] and Stephan Roche[*,†,#]

[†]Catalan Institute of Nanotechnology, CIN2 (ICN-CSIC) and Universitat Autónoma de Barcelona, Campus UAB, 08193 Bellaterra, Spain

[§]Department of Physics, University of Vienna, Boltzmanngasse 5, 1090 Wien, Austria

[∥]Department of Physics, University of Helsinki, P.O. Box 43, 00014 University of Helsinki, Finland

[⊥]Ecole Normale Superieure de Lyon, 46, Allée d'Italie, 69007 Lyon, France

[#]ICREA, Institució Catalana de Recerca i Estudis Avançats, 08070 Barcelona, Spain

ABSTRACT: Polycrystalline graphene is a patchwork of coalescing graphene grains of varying lattice orientations and size, resulting from the chemical vapor deposition (CVD) growth at random nucleation sites on metallic substrates. The morphology of grain boundaries has become an important topic given its fundamental role in limiting the mobility of charge carriers in polycrystalline graphene, as compared to mechanically exfoliated samples. Here we report new insights to the current understanding of charge transport in polycrystalline geometries. We created realistic models of large CVD-grown graphene samples and then computed the corresponding charge carrier mobilities as a function of the average grain size and the coalescence quality between the grains. Our results reveal a remarkably simple scaling law for the mean free path and conductivity, correlated to atomic-scale charge density fluctuations along grain boundaries.

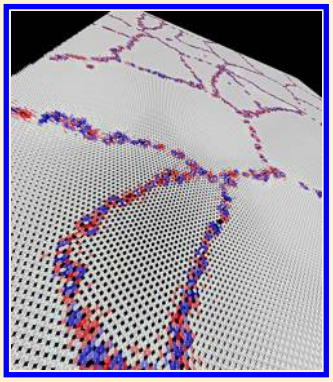

KEYWORDS: *Polycrystalline graphene, grain boundaries, charge transport, mobility*

The properties of polycrystalline materials are dictated by their grain size and by the atomic structure at the grain boundaries. These effects are particularly pronounced in low-dimensional materials, such as graphene.[1] This topic is of current technological relevance since chemical vapor deposition (CVD) growth of graphene on metallic substrates[2−5] is simultaneously initiated at different nucleation sites, which leads to samples with randomly distributed grains of varying lattice orientations.[6] As a result, grain boundaries (GB) dictate the electrical transport performance in CVD-graphene.[7]

Effects of structural defects on the electronic, mechanical, and transport properties of graphene have recently been analyzed theoretically.[8,9] Moreover, several theoretical studies have reported on the effect of a single GB on electronic,[10,11] magnetic,[12] chemical,[13] and mechanical[14−16] properties of graphene. However, very few studies[13,16] have discussed more complex forms of GBs (not restricted to infinite linear arrangements of dislocation cores), which would better correspond to the experimentally observed structures.[6,17,18]

Due to experimental challenges, only a few experimental works[19] have systematically investigated the impact of grain boundaries on electronic transport, mainly confirming the reduced conductivity as compared to single-crystalline samples. Very recent electrical measurements on individual grain boundaries in CVD-graphene also reported that a good interdomain connectivity is a fundamental geometrical requirement for improved transport capability.[20] However, to date little is known about the global contribution of complex distributions of GBs to measured charge mobilities.[21]

Here, we provide a comprehensive theoretical picture of the relationship between a polycrystalline morphology and the resulting charge transport properties. We explored large models (up to 278 000 atoms) of polycrystalline graphene samples with varying misorientation angles, realistic carbon ring size statistics, and nonrestricted GB structures. For this purpose, we used an efficient computational approach that is particularly well suited for large samples of low-dimensional systems.[22] We calculated charge mobilities in these samples using a tight-binding (TB) Hamiltonian and an efficient real space (order-N) quantum transport method, which enabled us to establish a surprisingly simple scaling law for transport properties for samples with well interconnected grains. The law relates the mean free path and conductivity of the sample to its average grain size. This scaling property is inferred from the observed electron−hole density fluctuations that develop at the atomic scale along the boundaries. For poorly connected samples, we observed greatly reduced mobilities, which agrees with experimental results.[20] These findings offer unprecedented insight into the transport fingerprints of polycrystalline graphene samples.

Received: January 25, 2013
Revised: February 27, 2013
Published: February 28, 2013

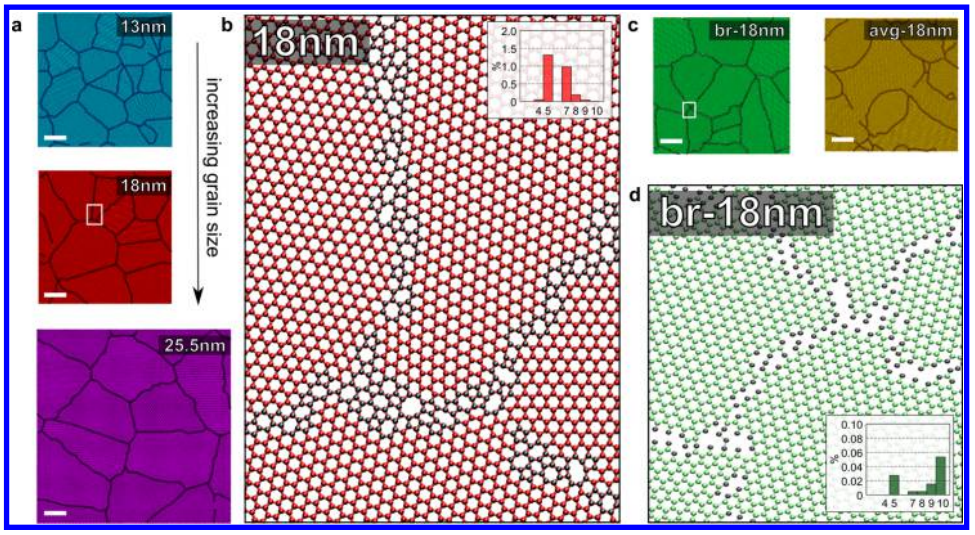

Figure 1. (a) Three structures with uniform grain size distribution and increasing average grain sizes (13.0, 18.0, and 25.5 nm). GBs are marked with dark lines. (b) Larger magnification of the area marked with a white rectangle in panel a, showing a typical example of the grain boundaries. Carbon ring-size statistics for the same sample (showing the ratio of nonhexagonal rings) are presented in the upper right corner. (c) Two additional samples with average grain size of 18 nm: one sample with broken boundaries ("br-18 nm") and another one with random grain size distribution ("avg-18 nm"). (d) Higher magnification of the area marked with a white rectangle in panel c, showing the structure of "broken" boundaries in sample "br-18 nm". The statistics of nonhexagonal rings are shown in the lower right corner. All scale bars are 10 nm.

Our model structures were created using the method outlined in ref 16: (1) Nucleation sites for a selected number of randomly oriented graphene grains are randomly placed on a predefined two-dimensional simulation cell; (2) Atoms are randomly added to the reactive sites at the edges of the grains until two grains meet, at which point the growth is locally terminated; (3) When no reactive sites are free, the structure is heated to 3000 K for 50 ps within a molecular dynamics simulation to allow the grain boundary structures to overcome the most spurious atomic configurations; (4) The structure is quenched during a 10 ps simulation run to enable the lattice to obtain its equilibrium size (zero pressure). Since a prerequisite to the efficient calculation of electronic properties in this study was that the structures had to be flat, at this point, we removed small corrugations which appeared after the aforementioned preparation steps. To this end, the structures were repeatedly stretched, gradually forced toward zero in the third dimension (by scaling down the z-coordinates), and again relaxed (allowing atomic reconstruction at each step), which removed the largest portion of nonflat configurations. A few remaining nonflat and physically implausible configurations (overlapping atoms, coordination numbers higher than 3) were removed manually, and a final relaxation and optimization step was carried out. This resulted in flat structures occupying local energy minima and suitable for the present study.

During the sample preparation, the carbon−carbon interactions were modeled using the reactive bond order potential by Brenner et al.[30] and the temperature and pressure control were handled using the Berendsen method.[31] Most of the structures were approximately 60 × 60 nm^2 in size and contained ∼138 000 atoms with the exception of one structure which was significantly larger (87 × 87 nm^2, ∼278 000 atoms). Structure with the smallest grains contained 22 of them, whereas all other structures contained 11 grains. Periodic boundaries were used in all calculations.

For electronic and transport calculations, we used a $\pi-\pi^*$ orthogonal TB model, described by a single p_z-orbital per carbon site, with nearest neighbors hopping γ_0 and zero onsite energies. A distance criterion to search for the first nearest neighbors was set empirically to 1.15 × a_{CC}, where a_{CC} is the nearest neighbor distance in pristine graphene. The local fluctuations in bond lengths are small enough to keep a constant value of γ_0 for the transfer integral. The density of states (DOS) was computed using the Lanczos recursion method with N = 1000 recursion steps and an energy resolution $\eta = 0.01\gamma_0 \simeq 0.03$ eV. For LDOS calculations we used the spectral measure operator $\delta(E - \hat{\mathcal{H}})$ projected on state $|i\rangle$ (where i is the site index).

We computed the local charge density deficiency δ_i (or self-doping) for each GB site i defined as:

$$\delta_i = \int_{-\infty}^{E_{CNP}} [\rho_{tot}(E) - \rho_i(E)]dE \quad (1)$$

where ρ_{tot} and ρ_i are the total DOS (per carbon atom) of the polycrystalline graphene sample and the LDOS on carbon site i, respectively. E_{CNP} denotes the charge neutrality point.

To capture the different transport regimes, we employed a real-space order-N quantum wavepacket evolution approach to compute the Kubo−Greenwood conductivity,[22,23] from which the zero-frequency conductivity for carriers at energy E is given by

$$\sigma_{dc} = e^2\rho(E)\lim_{t\to\infty}\frac{d}{dt}\Delta X^2(E, t) \quad (2)$$

where $\rho(E)$ is the density of states and $\Delta X^2(E,t)$ is the mean quadratic displacement of the wave packet at energy E and time t:

$$\Delta X^2(E, t) = \frac{\mathrm{Tr}[\delta(E - \mathcal{H})|\hat{X}(t) - \hat{X}(0)|^2]}{\mathrm{Tr}[\delta(E - \mathcal{H})]} \quad (3)$$

from which the diffusion coefficient $D_x(E,t) = d/dt(\Delta X^2(E,t))$ contains all information about multiple scattering effects, providing the quantum conductivity in the long time limit through eq 2. Assuming an isotropic system in x- and y-directions, the 2D diffusion coefficient becomes $D(t) = D_x(t)$ +

dx.doi.org/10.1021/nl400321r | Nano Lett. 2013, 13, 1730−1735

$D_y(t) = 2D_x(t)$. $D(t)$ always starts with a short-time ballistic motion followed by a saturation value ($D^{max}(E)$), from which semiclassical quantities (elastic mean free path $l_e(E)$ and the semiclassical conductivity σ_{sc}) are estimated as $l_e(E) = D^{max}(E)/2v(E)$ and $\sigma_{sc}(E) = 1/4(e^2\rho(E)D^{max}(E))$, respectively (with $v(E)$ being the carrier velocity). When disorder is strong enough, $D_x(E,t)$ decays as a result of quantum interferences, the strength of which will either drive the electronic system to weak localization or to the strong Anderson localization regime.

As has been shown before,[16] our models for polycrystalline graphene resemble experimentally observed structures: atomic-resolution and diffraction-filtered electron microscopy experiments have revealed that the grains stitch together predominantly via pentagon–heptagon pairs[6,17,18] in arrangements of large number of small grains forming an intricate patchwork interconnected by tilt boundaries.[6,18] For this study, we created samples with three different average grain sizes (average diameter $\langle d \rangle \approx 13$, 18, and 25.5 nm) and uniform grain size distributions (Figure 1a). As seen in Figure 1b, the atomic structure at the GBs consists predominantly of five- and seven-membered carbon rings and assumes meandering shapes similar to the experimentally observed ones. We also created one sample with $\langle d \rangle \approx 18$ nm and "broken" (poorly connected) boundaries ("br-18 nm"), and one sample with $\langle d \rangle \approx 18$ nm and nonuniform d-distribution ("avg-18 nm") (see Figure 1c,d).

We begin by discussing the electronic density of states (DOS) as a function of energy (E) for the different samples (Figure 2a). We noticed very little variation away from the charge neutrality point ($E = 0$), except for a slight broadening of van Hove singularities at $E = \pm \gamma_0$, where $\gamma_0 = -2.9$ eV is the nearest neighbor hopping energy. This suggests that GBs induce weak disorder and that the polycrystalline samples mostly preserve the electron–hole symmetry. However, a larger difference can be seen at the charge neutrality point (Figure 2b), where all of the polycrystalline structures show an enhanced density of zero energy modes.[24] As expected, the largest difference relative to pristine graphene was observed with the "br-18 nm" sample (the one with poorly connected grains), reflecting a higher density of "midgap" states.[24,25]

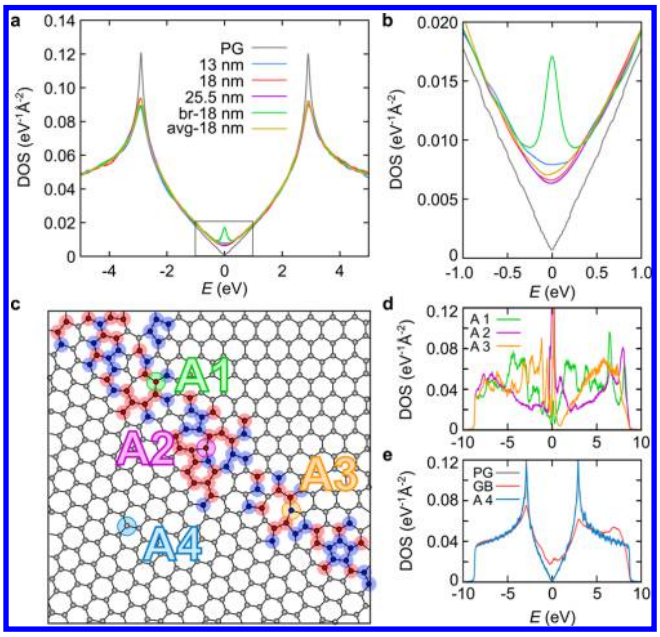

Figure 2. (a) DOS for pristine graphene (PG) and the structures presented in Figure 1. (b) Higher magnification of the DOS close to the charge neutrality point ($E = 0$, area marked with a rectangle in panel a). (c) Atomic structure of one of the boundaries in sample "18 nm", showing the electron–hole density fluctuations at GB sites that develop due to local variations in the charge density δ_i: local electron doping ($\delta_i < -1 \times 10^{-4}$ e/atom) is shown in blue and local hole doping ($\delta_i > 1 \times 10^{-4}$ e/atom) in red. (d) Local DOS for atoms A1, A2, and A3 marked in panel c. (e) Local DOS for atom A4 marked in panel c as compared to the average DOS for pristine graphene (PG) and average LDOS for all atoms at GBs in the same sample (GB).

To better understand the deviations from the pristine graphene for the well-connected structures, we next identified atoms residing at GBs of the "18 nm" sample by searching for atoms for which the bond length of at least one nearest neighbor differs from the carbon spacing in pristine graphene ($a_{CC} = 1.42$ Å) by 0.03 Å or more. We then calculated the local charge density deficiency δ_i (or self-doping) for each GB site. In Figure 2c we present the atomic structure of the electron–hole density fluctuations (δ_i variations greater than 10^{-4} electrons per atom) formed at a small area around one GB. These self-doping effects stem from local fluctuations in the electrostatic potential. Experiments on exfoliated graphene deposited over silicon dioxide[26,27] have shown similar potential inhomogeneities; however, these were spread over a much longer scale (~30 nm) and were induced by proximity effects generated by charges trapped in the oxide. In our case, averaging over all carbon atoms belonging to the grain boundaries of the 18 nm sample gave $\langle \delta \rangle_{GB} = 0.008$ electrons per atom, which corresponds to a mean carrier density of $\langle n(E = 0) \rangle \simeq 6.1 \times 10^{11}$ cm^{-2}. (δ fluctuates between −0.096 and 0.08 electrons per carbon atom, or, respectively, 6.1×10^{12} and -7.3×10^{12} cm^{-2}.) The local charge density fluctuations occur on a length scale only a few times larger than the lattice spacing, which is very small compared to that in supported exfoliated graphene, suggesting a much stronger local scattering efficiency. We point out that our results show no straightforward correlation between the self-doping value and the local defected morphology of the lattice.

Figure 2d shows the plot of the corresponding local DOS (LDOS) of three selected atoms at the boundary (A1, A2, and A3). All of them show increased contributions of midgap states,[24,25] significantly reduced van Hove singularities, and a markedly enhanced electron–hole asymmetry, owing to the odd-membered carbon rings.[22] They also exhibit strong resonant peaks, which are characteristic of quasi-localized electronic states in the vicinity of defects. The local electronic configuration along the GB also strongly differs from one site to another, an effect arising from an interference effect between coherent wave functions of the connected adjacent grains. In clear contrast, an atom only four lattice vectors away from the boundary (A4) shows a LDOS nearly indistinguishable from that of the pristine graphene (Figure 2e). A comparison to the average LDOS calculated for *all* atoms at the GBs reveals that the changes in the DOS seen in the polycrystalline samples (Figure 2a) arise locally from the atomic configurations of the GBs itself.

Next, we discuss the transport properties of the samples. Figure 3a shows the time dependency of the diffusion coefficient $D(t)$ at the Dirac point for all samples. On the one hand, the well-connected samples display a very slow time-dependent decay of $D(t)$ after the saturation value, indicating weak contribution of quantum interferences. On the other

dx.doi.org/10.1021/nl400321r | Nano Lett. 2013, 13, 1730–1735

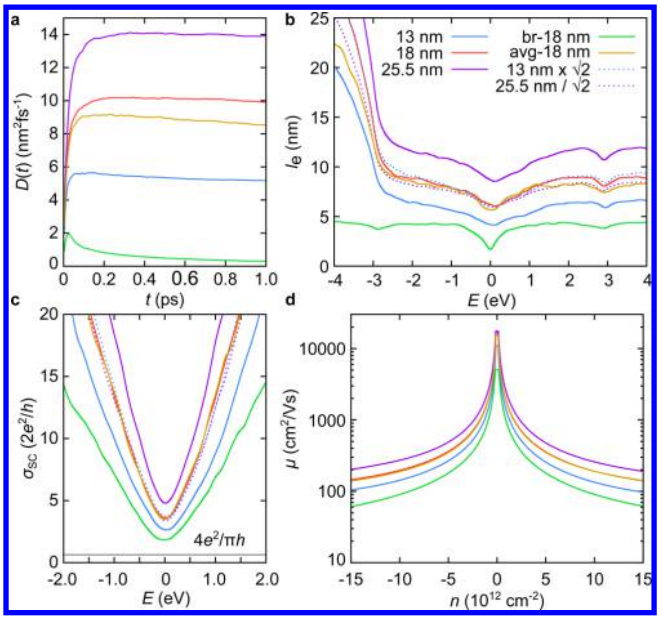

Figure 3. (a) Diffusion coefficient ($D(t)$) for the samples presented in Figure 1. (b) Mean free path $l_e(E)$ for equivalent structures with scaled $l_e(E)$ for samples with $\langle d\rangle \approx 13$ nm and $\langle d\rangle \approx 25.5$ nm, showing the scaling law. (c) Semiclassical conductivity ($\sigma_{sc}(E)$) for all samples and as scaled for the same cases as above. (d) Charge mobility ($\mu(E) = \sigma_{sc}(E)/en(E)$) as a function of the carrier density $n(E)$ in each of the samples ($n(E) = 1/S\int_0^E \rho(E)\mathrm{d}E$, S being a normalization factor).

hand, the poorly connected sample "br-18 nm" exhibits a much faster decay, eventually driving the electronic system to a strong localization regime (as observed in some transport measurements[19]). We next deduced the mean free path $l_e(E)$ from the maximum values of $D(t)$ (Figure 3b). Genuine electron−hole asymmetry is apparent in $l_e(E)$, but only for energies $|E|>3$ eV (far from the experimentally relevant energy window). At lower energies around the charge neutrality point ($|E| < 1$ eV), $l_e(E)$ changes, albeit only weakly, for all samples.

The sample with broken boundaries, "br-18 nm", shows the shortest $l_e < 5$ nm and the weakest dependence on energy, except for a pronounced dip at $E = 0$. Interestingly, the curves for the two well-connected samples with similar $\langle d\rangle$ but different d-distributions ("18 nm" and "avg-18 nm") are very similar and clearly different from samples with either smaller or larger grains. However, this difference can be accounted for by a constant factor. Remarkably, it turns out that $\sqrt{2} \times l_e^{13\ \mathrm{nm}} \approx l_e^{18\ \mathrm{nm}}$ and $\sqrt{2} \times l_e^{18\ \mathrm{nm}} \approx l_e^{25.5\ \mathrm{nm}}$ (see the scaled values in Figure 3b), which correspond exactly to the differences in the average grain sizes in these samples ($\sqrt{2} \times 13 \approx 18$ and $\sqrt{2} \times 18 \approx 25.5$). Moreover, the grain-size distribution does not enter into this scaling behavior ($l_e^{18\ \mathrm{nm}} \approx l_e^{\text{avg-18 nm}}$). Hence, we have identified a remarkably simple scaling law that links the average grain size to transport length scales in polycrystalline graphene with randomly oriented grains.

The computed semiclassical conductivity $\sigma_{sc}(E)$ exhibits energy-dependent variations similar to $l_e(E)$, as can be seen in Figure 3c. We also point out the linear dependency of σ_{sc} with charge density in the vicinity of the Dirac point. Again, the same scaling law (presented above for the mean free path) applies: the ratio of σ_{sc} for two samples with different average grain sizes matches closely with the ratio of the $\langle d\rangle$ values themselves. One additional interesting feature seen in Figure 3c is that the conductivity remains much higher than the minimum value $4e^2/\pi h$ (horizontal line), which fixes the theoretical limit in the diffusive regime, as derived within the self-consistent Born approximation valid for any type of disorder.[9] This indicates that polycrystalline graphene remains a good conductor, even for the poorly connected structure "br-18 nm".

Localization length of electron states ($\xi(E)$) can now be estimated using the values for l_e and σ_{sc}. Scaling analysis ($\xi(E) = l_e(E)\exp(\pi h\sigma_{sc}(E)/2e^2)$[28]) reveals that $\xi \simeq 1-10$ μm over a large energy window around the charge neutrality point. This contrasts with the values (on the order of 10 nm) obtained for graphene structures with ∼1% structural defects, strongly bonded adatoms, or other types of short-range impurities.[22,29]

Finally, we move on to the charge carrier mobility $\mu(n)$ (Figure 3d). As expected, the poorly connected sample "br-18 nm" shows the lowest mobility (reduced by a factor of about three when compared to the well-connected samples with similar $\langle d\rangle$). We point out that the computed values are valid down to the charge neutrality point (that is, to the smallest charge density $n(E)$), since we accounted for the disorder-induced finite DOS, which yields a nonzero charge density (and thus no singularity at $1/n(E)$). Table 1 gives the mobilities at several charge densities for all studied samples. It is worth observing that the scaling law also roughly applies to charge mobilities versus average grain size, since the superimposed effect of density of states changes the ratio only by a few percent (for instance, at $n = 2.5 \times 10^{12}$ cm^{-2}, $\mu^{18\ \mathrm{nm}}/\mu^{13\ \mathrm{nm}} \approx 1.37$).

If we extrapolate the mobility for well-connected grains according to our scaling law to a grain size of 1 μm and a charge density of $n = 3 \times 10^{11}$ cm^{-2} as in the best samples of ref 20, we obtain 300 000 cm^2 V^{-1} s^{-1}, which is about ten times higher than the measured values. This discrepancy suggests that substrate-related disorder effects, as well as supplementary defects introduced during the transfer process, should account for an even greater limitation for charge mobilities than the actual GB morphology.

The existence of more disordered grain boundaries as reported in refs 20 and 32 or samples with overlapping grains, as observed in ref 33 yield to lower mobility values, which has been partly illustrated here with the structural model "br-18 nm". More experimental data is however needed before proper atomistic structural models, capturing the essential geometrical features of those more fragmented structures of polycrystalline graphene, can be constructed.

In conclusion, we have created polycrystalline graphene samples with nonrestricted grain boundary structures and realistic misorientation angles and ring statistics. These samples enabled us to discover a simple relationship between the

Table 1. Mobilities for All Samples at Selected Charge Densities

mobilities (cm^2/(V s))	13 nm	18 nm	avg-18 nm	25.5 nm	br-18 nm
$\mu(n = 2.5 \times 10^{11}$ cm$^{-2})$	5.1×10^3	7×10^3	6.8×10^3	10^4	4×10^3
$\mu(n = 2.5 \times 10^{12}$ cm$^{-2})$	510	700	685	950	360
$\mu(n = 2.5 \times 10^{13}$ cm$^{-2})$	69	105	104	150	45

dx.doi.org/10.1021/nl400321r | Nano Lett. 2013, 13, 1730−1735

average grain size and charge transport properties. The disorder scattering strength in polycrystalline graphene was found to depend on the atomic structure of GBs (inducing quasi-bound states at resonant energy) and wave function mismatch between the grains, which generate strongly fluctuating, but highly localized electron−hole density fluctuations along the interfaces between grains. Our results significantly improve the present theoretical understanding on the influence of the detailed morphology of polycrystalline materials to their measurable electronic properties. They offer the possibility for estimating charge mobilities in suspended CVD-graphene samples based on the average grain sizes and quality of the GBs. Furthermore, they establish quantitative foundations for estimating the intrinsic limits of charge transport in polycrystalline graphene, which is of prime importance for graphene-based applications in the future.

AUTHOR INFORMATION

Corresponding Author

*E-mail: jani.kotakoski@iki.fi; stephan.roche@icn.cat.

Notes

The authors declare no competing financial interest.

ACKNOWLEDGMENTS

J.K. acknowledges computational resources from the Vienna Scientific Cluster and funding from University of Helsinki Funds as well as the Austrian Science Fund (FWF): M 1481-N20. S.R. acknowledges the support from SAMSUNG within the *Global Innovation Program*.

REFERENCES

(1) Geim, A. K.; Novoselov, K. S. The rise of graphene. *Nat. Mater.* **2007**, *6*, 183.

(2) Li, X. S.; Cai, W. W.; An, J. H.; Kim, S.; Nah, J.; Yang, D. X.; Piner, R.; Velamakanni, A.; Jung, I.; Tutuc, E.; Banerjee, S. K.; Colombo, L.; Ruoff, R. S. Large-Area Synthesis of High-Quality and Uniform Graphene Films on Copper Foils. *Science* **2009**, *324*, 1312−1314.

(3) Reina, A.; Jia, X.; Ho, J.; Nezich, D.; Son, H.; Bulovic, V.; Dresselhaus, M. S.; Kong, J. *Nano Lett.* **2009**, *9*, 30.

(4) Li, X. S.; Magnuson, C. W.; Venugopal, A.; An, J. H.; Suk, J. W.; Han, B. Y.; Borysiak, M.; Cai, W. W.; Velamakanni, A.; Zhu, Y. W.; Fu, L. F.; Vogel, E. M.; Voelkl, E.; Colombo, L.; Ruoff, R. S. Graphene Films with Large Domain Size by a Two-Step Chemical Vapor Deposition Process. *Nano Lett.* **2010**, *10*, 4328−4334.

(5) Bae, S.; Kim, H.; Lee, Y.; Xu, X. F.; Park, J. S.; Zheng, Y.; Balakrishnan, J.; Lei, T.; Kim, H. R.; Song, Y. I.; Kim, Y. J.; Kim, K. S.; Ozyilmaz, B.; Ahn, J. H.; Hong, B. H.; Iijima, S. Roll-to-roll production of 30-in. graphene films for transparent electrodes. *Nat. Nanotechnol.* **2010**, *5*, 574−578.

(6) Huang, P. Y.; Ruiz-Vargas, C. S.; van der Zande, A. M.; Whitney, W. S.; Levendorf, M. P.; Kevek, J. W.; Garg, S.; Alden, J. S.; Hustedt, C. J.; Zhu, Y.; Park, J.; McEuen, P. L.; Muller, D. A. Grains and grain boundaries in single-layer graphene atomic patchwork quilts. *Nature* **2011**, *469*, 389.

(7) Novoselov, K. S.; Falko, V. I.; Colombo, L.; Gellert, P. R.; Schwab, M. G.; Kim, K. A roadmap for graphene. *Nature* **2012**, *192*, 490.

(8) Krasheninnikov, A. V.; Banhart, F. Engineering of nanostructured carbon materials with electron or ion beams. *Nat. Mater.* **2007**, *6*, 723.

(9) Roche, S.; Leconte, N.; Ortmann, F.; Lherbier, A.; Soriano, D.; Charlier, J. C. Quantum transport in disordered graphene: a theoretical perspective. *Sol. Stat. Commun.* **2012**, *152*, 1404.

(10) Peres, N. M. R.; Guinea, F.; Castro-Neto, A. H. Electronic properties of disordered two-dimensional carbon. *Phys. Rev. B* **2006**, *73*, 125411.

(11) Yazyev, O. V.; Louie, S. G. Electronic transport in polycrystalline graphene. *Nat. Mater.* **2010**, *9*, 806.

(12) Cervenka, J.; Katsnelson, M. I.; Flipse, C. F. J. Room-temperature ferromagnetism in graphite driven by two-dimensional networks of point defects. *Nature Phys.* **2007**, *5*, 840.

(13) S. Malola, S.; Hakkinen, H.; Koskinen, P. Chemical and dynamical trends in graphene grain boundaries. *Phys. Rev. B* **2010**, *81*, 165447.

(14) Liu, Y.; Yakobson, B. I. Cones, pringles, and grain boundary landscapes in graphene topology. *Nano Lett.* **2010**, *10*, 2178.

(15) Grantab, R.; Shenoy, V. B.; Ruoff, R. S. Anomalous strength characteristics of tilt grain boundaries in graphene. *Science* **2010**, *330*, 946.

(16) Kotakoski, J.; Meyer, J. C. Mechanical properties of polycrystalline graphene based on a realistic atomistic model. *Phys. Rev. B* **2012**, *85*, 195447.

(17) Kurasch, S.; Kotakoski, J.; Lehtinen, O.; Skakalova, V.; Smet, J.; Krill, C. E.; Krasheninnikov, A. V.; Kaiser, U. Atom-by-atom observation of grain boundary migration in graphene. *Nano Lett.* **2012**, *12*, 3168.

(18) Kim, K.; Lee, Z.; Regan, W.; Kisielowski, C.; Crommie, M. F.; Zettl, A. Grain boundary mapping in polycrystalline graphene. *ACS Nano* **2011**, *5*, 2142.

(19) Yu, Q.; Jauregui, L.; Wu, W.; Colby, R.; Tian, J.; Su, Z.; Cao, H.; Liu, H.; Pandey, D.; Chung, D.; Peng, P.; Guisinger, N.; Stach, E.; Bao, J.; Pei, S.; Chen, Y. P. Control and characterization of individual grains and grain boundaries in graphene grown by chemical vapour deposition. *Nat. Mater.* **2011**, *10*, 443−449.

(20) Tsen, A. W.; Brown, L.; Levendorf, M. P.; Ghahari, F.; Huang, P. Y.; Havener, R. W.; Ruiz-Vargas, C. S.; Muller, D. A.; Kim, P.; Park, J. Tailoring electrical transport across grain boundaries in polycrystalline graphene. *Science* **2012**, *336*, 1143.

(21) Ferreira, A.; Xu, X.; Tan, C.-L.; Bae, S.; Peres, N. M. R.; Hong, B.-H.; Ozyilmaz, B.; Castro Neto, A. H. Transport properties of graphene with one-dimensional charge defects. *Eur. Phys. Lett.* **2011**, *94*, 28003.

(22) Lherbier, A.; Dubois, S. M.; Declerck, X.; Roche, S.; Niquet, Y.; Charlier, J. C. Two-dimensional graphene with structural defects: elastic mean free path, minimum conductivity, and Anderson transition. *Phys. Rev. Lett.* **2011**, *106*, 046803.

(23) Roche, S. *Phys. Rev. B* **1999**, *59*, 2284.

(24) Pereira, V. M.; Guinea, F.; Lopes dos Santos, J. M. B.; Peres, N. M. R.; Castro Neto, A. H. Disorder induced localized states in graphene. *Phys. Rev. Lett.* **2007**, *96*, 036801.

(25) Pereira, V. M.; Lopes dos Santos, J. M. B.; Castro Neto, A. H. Modeling disorder in graphene. *Phys. Rev. B* **2008**, *77*, 115109.

(26) Martin, J.; Akerman, N.; Ulbright, G.; Lohmann, T.; Smet, J. H.; von Klitzing, K.; Yacoby, A. Observation of electron-hole puddles in graphene using a scanning single-electron transistor. *Nat. Phys.* **2008**, *4*, 144.

(27) Hwang, E. H.; Adam, S.; Das Sarma, S. Carrier transport in two-dimensional graphene layers. *Phys. Rev. Lett.* **2007**, *98*, 18.

(28) Evers, F.; A.D. Mirlin, A. D. Anderson transitions. *Rev. Mod. Phys.* **2008**, *80*, 1355.

(29) Radchenko, T. M.; Shylau, A. A.; Zozoulenko, I. V. Influence of correlated impurities on conductivity of graphene sheets: time-dependent real-space Kubo approach. *Phys. Rev. B* **2012**, *86*, 035418.

(30) Brenner, D. W.; Shenderova, O.; Harrison, J.; Stuart, S.; Ni, B.; Sinnott, S. A second-generation reactive empirical bond order (REBO) potential energy expression for hydrocarbons. *J. Phys.: Condens. Matter* **2002**, *14*, 783.

(31) Berendsen, H.; Postma, P. M.; Gunsteren, W.; DiNola, A.; Haak, J. Molecular dynamics with coupling to an external bath. *J. Chem. Phys.* **1984**, *81*, 3684.

(32) Tapaszto, L.; Nemes-Incze, P.; Dobrik, G.; Yoo, K. J.; Hwang, Ch.; Biro, L. P. Mapping the electronic properties of individual graphene grain boundaries. *Appl. Phys. Lett.* **2012**, *100*, 053114.
(33) Robertson, A. W.; Bachmatiuk, A.; Wu, Y. A.; Schäffel, F.; Rellinghaus, B.; Büchner, B.; Rümmeli, M. H.; Warner, J. H. Atomic Structure of Interconnected Few-Layer Graphene Domains. *ACS Nano* **2011**, *5*, 6610.